



# Dynamics of coupled reacted flow of Oldroyd-B material induced by isothermal/exothermal stretched disks with Joule heating, viscous dissipation and magnetic dipoles



M. Sadiq Hashmi <sup>a</sup>, Nargis Khan <sup>b</sup>, Sami Ullah Khan <sup>c</sup>, M. Ijaz Khan <sup>d</sup>,  
Niaz B. Khan <sup>e</sup>, Mubbashar Nazeer <sup>f</sup>, Seifedine Kadry <sup>g</sup>, Yu-Ming Chu <sup>h,i,\*</sup>

<sup>a</sup> Department of Mathematics, The Islamia University of Bahawalpur, Bahawalpur 63100, Pakistan

<sup>b</sup> Department of Mathematics, The Govt. Sadiq College Women University, Bahawalpur, Pakistan

<sup>c</sup> Department of Mathematics, COMSATS University Islamabad, Sahiwal 57000, Pakistan

<sup>d</sup> Department of Mathematics and Statistics, Riphah International University, I-14, Islamabad 44000, Pakistan

<sup>e</sup> School of Mechanical and Manufacturing Engineering, National University of Sciences and Technology, Islamabad, Pakistan

<sup>f</sup> Department of Mathematics, Institute of Arts and Science, Government College University Faisalabad, Chiniot Campus, Pakistan

<sup>g</sup> Department of Mathematics and Computer Science, Beirut Arab University, Beirut, Lebanon

<sup>h</sup> Department of Mathematics, Huzhou University, Huzhou 313000, PR China

<sup>i</sup> Hunan Provincial Key Laboratory of Mathematical Modeling and Analysis in Engineering, Changsha University of Science & Technology, Changsha 410114, PR China

Received 2 September 2020; revised 27 September 2020; accepted 7 October 2020

Available online 21 October 2020

## KEYWORDS

Oldroyd-B fluid;  
Joule dissipation;  
Magnetic dipoles;  
Stretching disks;  
Homotopy analysis method

**Abstract** Current investigation presents the heat and mass transfer analysis for steady flow Oldroyd-B fluid induced by isothermally and exothermally stretching disks. The novel features of Joule heating, chemical reaction and Ohmic dissipations are also utilized in the energy and concentration equations. A non-dimensional set of transformations are introduced to convert the coupled partial differential system into a system of ordinary differential equations. The analytical solution of formulated dimensionless equations is obtained by using homotopy analysis method. The solution convergence is ensured carefully. The physical exploration of various dimensionless parameters on pressure, velocity, temperature and concentration profiles is presented. It is observed that heat transfer at lower disk increases with increment of Deborah number, Archimedes number and distance parameter. The rate of mass transfer at both surfaces of disk is enhanced for larger values of activation energy parameter and Deborah number.

© 2020 The Authors. Published by Elsevier B.V. on behalf of Faculty of Engineering, Alexandria University. This is an open access article under the CC BY-NC-ND license (<http://creativecommons.org/licenses/by-nc-nd/4.0/>).

\* Corresponding author at: Department of Mathematics, Huzhou University, Huzhou 313000, PR China.

E-mail address: [chuyuming@zjhu.edu.cn](mailto:chuyuming@zjhu.edu.cn) (Y.-M. Chu).

Peer review under responsibility of Faculty of Engineering, Alexandria University.

## 1. Introduction

In recent century, the dynamic investigators have focused their attention to explore the complex behavior of non-Newtonian liquids due to their practical involvement in many chemical, mechanical and processing industries. On this end, numerous diverse mathematical relationships have been suggested in the past to elaborate the actual response of such nano-Newtonian materials. The general classification of such materials is characterized into rate type, integral type and differential type. The mechanisms of shear thickening/thinning impacts can be evaluated by second or third grade liquid models. The theory of stress retardation and relaxation cannot be deliberated by the differential constitutive relationships. The simplest model to predict extra stress relaxation phenomenon is known as Maxwell fluid which belong to the class of rate type model. The literature on Maxwell liquid model can be referred to refs. [1–8]. Another rate type non-Newtonian materials is Oldroyd-D fluid which have also intended the researchers attention. The impacts of memory and elastic can be visualized by an Oldroyd-B non-Newtonian liquid model. The properties of stress retardation and relaxation can be evaluated through this model. The most of the polymers and biological liquids are characterized as Oldroyd-B liquid and has pivotal applications in biomedical and environmental engineering fields. Some attempts on Oldroyd-B liquid can be seen in [9–11].

The coupled forced and free convective flows generally known as “mixed convection flows” and have wider application in many industries which include electronic devices cooling, energy storage, furnaces, lubrication technologies, astrophysics processes, geology, chemical and transport processes, drying, fire control, food industries, refrigerators and metallurgy. The liquid temperature difference of two isothermal plates is called free convection while the heat flow induced by some externally applied force is known as forced convective flow. The consideration of buoyancy terms lead to complicated mathematical model because the transport of liquid and thermal properties become coupled. The flow due to mixed convection has involvement of Archimedes number ( $Gr/Re^2$ ) which describes the contribution of forced and natural convection. The free convective flow dominates over forced convective flow when Archimedes number is more dominant. A number of investigations have been done on the phenomenon of flows generated by heat supplied in which the transport processes are encountered due to chemical reactions. The flows due to such chemical reaction are formulated through the use of Arrhenius kinetics theory [12–20]. Minto et al. [21] and Merkin and Mahmood [22,23] examined the reactive surfaces flows through porous media. According to the literature in spatial manner [24], flow along with chemical reaction was confined to the condition; however, our interest is to investigate the chemical reaction which occurs along boundaries and surface of flow regime. Further, heat absorption and generation phenomenon is very spatial to controlling the heat transport in industrial processes. Srinivas et al. [25] reported the role of space porosity and solar radiation in MHD convective flow of viscous liquid induced by channel having vertical walls. The importance of heat sink and source in Maxwell liquid

by suspended nanoparticles addressed Ramesh et al. [26]. Few important studies on heat source/sink can be viewed in [27–29].

The investigation of MHD flows generated by stretched disks play a superficial role in polymer industry, physics, metallurgy and many engineering problems. The interaction of electrically conducting liquid and magnetic field serious effected much industrial equipment such as MHD generators, pumps and bearing sand. An electrically conducting fluid subject to magnetic dipole plays a significant role in controlling the fluid temperature and control the rate of cooling of final product. The research on MHD flow has also important in physiological problems like machines of blood pump and blood plasma. Hayat et al. [30] investigates the interaction of Lorentz force in flow of Maxwell nano-liquid with convective heat transport. Waqas et al. [31] explore the magnetohydrodynamic features in magnetized flow of Carreau-Yasuda nanofluid in presence of gyrotactic microorganisms. Malik et al. [32] focused on MHD flow of tangent hyperbolic fluid over a stretching cylinder. Mahanthesh et al. [33] intended the concept of Lorentz and Coriolis forces in magnetohydrodynamic flow of nanofluid induced by a radially moving disk. The stretched flow for Carreau non-Newtonian material under the specified influence of magnetic force was numerically elaborated by Mahanthesh [34]. Gireesha and co-researchers [35] discussed the Hall and heat consumption and generation consequences in MHD flow of dusty nano-material. The numerical inspection regarding rotating flow of nanofluid under the novel impact of magnetic force, thermal radiation and heat generation features was visualized by Mahanthesh et al. [36]. In another investigation Mahanthesh et al. [37] analyzed the MHD flow of nanofluid configured by a rotating disk. The irregular heat generation and absorption pattern was followed to improve the heat transportation process.

The basic theme of the present research is to investigate the simultaneous impacts of magnetic dipole and chemical compositions in MHD mixed convection flow of Oldroyd-B liquid isothermally and exothermally stretching disks. At the lower disk surface, the Arrhenius kinetics process is maintained while upper disk has uniform concentration and temperature distributions. The study also elaborates the effect of exothermic reaction and Joule heating. The results from current analysis may involve many interesting applications in disk shaped surfaces like marine turbine, rotating heat exchangers, electronic devices, disk reactor for bio-fluids production, rotating wafers etc. According to available literature, no such attempt is available in the literature with similar flow features. A famous homotopy analysis scheme is employed to find the solution of coupled highly nonlinear formulated equation [38–41].

## 2. Problem formulation

Let us consider a simultaneous effects of heat and mass transfer in MHD flow of Oldroyd-B fluid induced in presence of magnetic dipole. The induced flow is referred to stretched disks that are separated by a distance  $d$ . The upper disk has uniform temperature and concentration while the lower disk has

exothermic reaction. It is assumed that both disks are stretched in radial direction. The energy equation is modified by using relations of Joule heating, viscous dissipation and exothermic reaction. The exothermic reaction expression through first order non-isothermal reaction (Merikin et al. [17]):

$$A \rightarrow B + \text{heat, rate} = k_0 a e^{-E/R_1 T}. \quad (1)$$

The above relations are known as Arrhenius kinetics where  $R_1$  is the constant of universal gas,  $B$  is product species,  $E$  is activation energy,  $k_0$  reflects the rate constant,  $a$  is concentration of reactant  $B$  while  $T$  is temperature. Due to axisymmetry, the azimuthal component of velocity vanishes and all quantities are independent of  $\theta$ . The resulting flow expressions for Oldroyd-B liquid are [11,39,40]:

$$\frac{1}{r} \frac{\partial}{\partial r} (ru) + \frac{\partial w}{\partial z} = 0, \quad (2)$$

$$\begin{aligned} u \frac{\partial u}{\partial r} + w \frac{\partial w}{\partial z} &= -\frac{1}{\rho} \frac{\partial p}{\partial r} + v \left( 2 \frac{\partial^2 u}{\partial r^2} + \frac{\partial^2 w}{\partial r \partial z} + \frac{\partial^2 u}{\partial z^2} + \frac{2}{r} \frac{\partial u}{\partial r} - 2 \frac{u}{r^2} \right) \\ &\quad - \lambda'_1 \left( w^2 \frac{\partial^2 u}{\partial z^2} + 2uw \frac{\partial^2 u}{\partial r \partial z} + u^2 \frac{\partial^2 u}{\partial r^2} \right) \\ &\quad + v \lambda'_2 \left( \frac{4u^2}{r^3} - \frac{2w}{r^2} \frac{\partial u}{\partial z} - \frac{1}{r} \left( \frac{\partial u}{\partial z} \right)^2 - 2 \frac{\partial u}{\partial z} \frac{\partial^2 w}{\partial z^2} + w \frac{\partial^3 u}{\partial z^3} \right. \\ &\quad \left. - \frac{2u}{r^2} \frac{\partial u}{\partial r} - \frac{\partial^2 u}{\partial z^2} \frac{\partial u}{\partial r} - \frac{2}{r} \left( \frac{\partial u}{\partial r} \right)^2 - \frac{1}{r} \frac{\partial u}{\partial z} \frac{\partial w}{\partial r} + \frac{2w}{r} \frac{\partial^2 u}{\partial r \partial z} \right. \\ &\quad \left. - \frac{\partial u}{\partial z} \frac{\partial^2 w}{\partial r \partial z} - \frac{\partial u}{\partial r} \frac{\partial^2 w}{\partial r \partial z} + u \frac{\partial^3 u}{\partial r \partial z^2} + w \frac{\partial^3 w}{\partial r \partial z^2} \right. \\ &\quad \left. + \frac{2u}{r} \frac{\partial^2 u}{\partial r^2} - 2 \frac{\partial u}{\partial r} \frac{\partial^2 u}{\partial r^2} - \frac{\partial u}{\partial z} \frac{\partial^2 w}{\partial r^2} + 2w \frac{\partial^3 u}{\partial r^2 \partial z} \right. \\ &\quad \left. + u \frac{\partial^3 w}{\partial r^2 \partial z} + 2u \frac{\partial^3 u}{\partial r^3} \right) + \frac{\sigma B_0^2}{\rho} \left( -u - \lambda'_1 w \frac{\partial u}{\partial z} \right) \\ &\quad + g \beta \left( (T - T_0) + \lambda'_1 \left( u \frac{\partial T}{\partial r} + w \frac{\partial T}{\partial z} - \frac{\partial u}{\partial r} (T - T_0) \right) \right), \end{aligned} \quad (3)$$

$$\begin{aligned} u \frac{\partial w}{\partial r} + w \frac{\partial w}{\partial z} &= -\frac{1}{\rho} \frac{\partial p}{\partial z} \\ &\quad + v \left( \frac{\partial^2 w}{\partial r^2} + \frac{\partial^2 u}{\partial r \partial z} + 2 \frac{\partial^2 w}{\partial z^2} + \frac{1}{r} \frac{\partial w}{\partial r} + \frac{1}{r} \frac{\partial u}{\partial r} \right) \\ &\quad - \lambda'_1 \left( w^2 \frac{\partial^2 w}{\partial z^2} + 2uw \frac{\partial^2 w}{\partial r \partial z} + u^2 \frac{\partial^2 w}{\partial r^2} \right) \\ &\quad + v \lambda'_2 \left( -\frac{u}{r^2} \frac{\partial u}{\partial z} - \frac{1}{r} \frac{\partial u}{\partial z} \frac{\partial w}{\partial z} + \frac{w}{r} \frac{\partial^2 u}{\partial z^2} \right. \\ &\quad \left. - 2 \frac{\partial w}{\partial z} \frac{\partial^2 w}{\partial z^2} + 2w \frac{\partial^3 w}{\partial z^3} + \frac{u}{r^2} \frac{\partial w}{\partial r} - \frac{1}{r} \frac{\partial w}{\partial r} \frac{\partial w}{\partial z} \right. \\ &\quad \left. - \frac{\partial^2 u}{\partial z^2} \frac{\partial w}{\partial r} - \frac{2}{r} \frac{\partial u}{\partial r} \frac{\partial w}{\partial r} + \frac{u}{r} \frac{\partial^2 u}{\partial r \partial z} - \frac{\partial w}{\partial z} \frac{\partial^2 u}{\partial r \partial z} \right. \\ &\quad \left. + \frac{w}{r} \frac{\partial^2 w}{\partial r \partial z} - \frac{\partial w}{\partial r} \frac{\partial^2 w}{\partial r \partial z} + w \frac{\partial^3 u}{\partial r \partial z^2} + 2u \frac{\partial^3 w}{\partial r \partial z^2} \right. \\ &\quad \left. - 2 \frac{\partial w}{\partial r} \frac{\partial^2 u}{\partial r^2} + \frac{u}{r} \frac{\partial^2 w}{\partial r^2} - \frac{\partial w}{\partial z} \frac{\partial^2 w}{\partial r^2} + u \frac{\partial^3 u}{\partial r^2 \partial z} \right. \\ &\quad \left. + w \frac{\partial^3 w}{\partial r^2 \partial z} + u \frac{\partial^3 w}{\partial r^3} \right) - g \beta \lambda'_1 (T - T_0) \frac{\partial w}{\partial r}, \end{aligned} \quad (4)$$

$$\begin{aligned} \rho c_p \left( u \frac{\partial T}{\partial r} + w \frac{\partial T}{\partial z} \right) &= \mu \left( 2 \left( \frac{\partial u}{\partial r} \right)^2 + \left( \frac{\partial u}{\partial z} \right)^2 + 2 \left( \frac{\partial w}{\partial r} \right) \left( \frac{\partial u}{\partial z} \right) \right. \\ &\quad \left. + 2 \left( \frac{u}{r} \right)^2 + \left( \frac{\partial w}{\partial r} \right)^2 + 2 \left( \frac{\partial w}{\partial z} \right)^2 \right) + K_T \left( \frac{\partial^2 T}{\partial r^2} + \frac{1}{r} \frac{\partial T}{\partial r} + \frac{\partial^2 T}{\partial z^2} \right) \\ &\quad + \sigma B_0^2 u^2 + Q k_0 a_0 e^{-E/R_1 T}, \end{aligned} \quad (5)$$

$$u \frac{\partial C}{\partial r} + w \frac{\partial C}{\partial z} = D \left( \frac{\partial^2 C}{\partial r^2} + \frac{1}{r} \frac{\partial C}{\partial r} + \frac{\partial^2 C}{\partial z^2} \right) - k C \quad (6)$$

In above equations  $u$  and  $w$  represents the components of velocity in  $r$  and  $z$  directions, respectively,  $p$  is the liquid pressure,  $\rho$  denotes characteristic density,  $v$  is kinematic viscosity,  $K_T$  symbolize the thermal conductivity,  $\lambda_1, \lambda_2$  are Deborah numbers of relaxation and retardation times respectively,  $T_0$  is the mean temperature and  $Q$  is exothermicity factor. The boundary conditions for current flow model are [11,39,40]

$$\begin{aligned} u &= ar, w = 0, p = \frac{a \mu \beta_1 r^2}{4d^2}, atz = 0, \\ u &= cr, w = 0, p = 0, atz = d, \\ K_T \frac{\partial T}{\partial z} &= -Q k_0 C_0 e^{-E/R_1 T} atz = 0, T = T_2 atz = d, \end{aligned} \quad (7)$$

$$D \frac{\partial C}{\partial z} = k_0 (C - C_0) e^{-E/R_1 T} atz = 0, C = C_2 atz = d$$

In order to reduce governing partial differential equations (1)-(6) into ordinary systems, the suggested similarity variables are [11,39,40]:

$$\begin{aligned} u &= ar F(\eta), w = ad H(\eta), p = a \mu \left( P(\eta) + \frac{\beta r^2}{4d^2} \right), \eta = \frac{z}{d}, \\ \theta(\eta) &= \frac{E(T - T_0)}{RT_0^2}, \varphi(\eta) = \frac{C - C_0}{C_2 - C_1}. \end{aligned} \quad (8)$$

The transformed flow problem is governed by following equations

$$\begin{aligned} \frac{R}{4} (H'^2 - 2HH'') &= -\frac{1}{2} \left[ \beta + H'' + \lambda_1 R (HH'H'' - H^2 H'') + \lambda_2 (HH^{(iv)} - H''^2) \right] \\ &\quad + \frac{RA_e \epsilon}{2\delta^4} (2\theta + \lambda_1 (H'\theta + 2H\theta')) + \frac{RM}{2} (H' + \lambda_1 (HH'')), \end{aligned} \quad (9)$$

$$\begin{aligned} \theta'' - RPr H\theta' + \frac{EcPr}{\epsilon} \left( \frac{\delta^2}{2} H''^2 + 3H'^2 - \frac{RM\delta^2}{4} H'^2 \right) \\ + Ke \left( \frac{-1}{\epsilon(1+\epsilon\theta)} \right) = 0, \end{aligned} \quad (10)$$

$$\varphi'' - Sc(RH\varphi' + \xi\varphi + \chi) = 0, \quad (11)$$

$$\begin{aligned} P' &= \frac{3H''}{2} - \frac{\delta H'}{2} - RHH' - R\lambda'_1 H^2 H'' \\ &\quad + \lambda'_2 \left( \frac{3}{2} H'H'' - 2HH'' + HH''' \right), \end{aligned} \quad (12)$$

with boundary conditions

$$H(0) = 0, H(1) = 0, H'(0) = -2, H'(1) = -2\gamma, P(0) = 0,$$

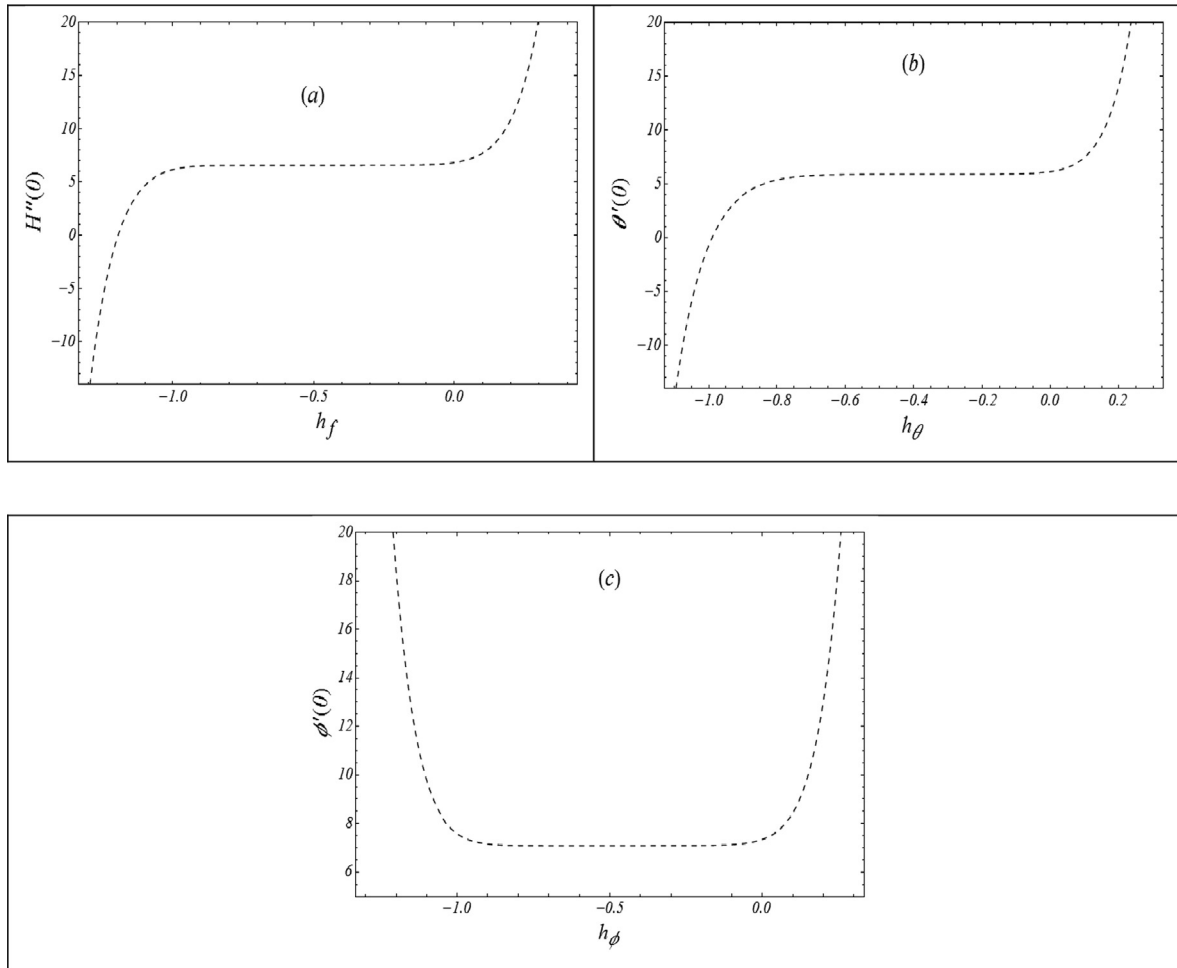


**Fig. 1** The  $h$ -curves of HAM solution for velocity, temperature and concentration profiles when  $R = 0.1$ ,  $\gamma = 0.1$ ,  $M = 0.2$ ,  $A_r = 0.2$ ,  $\delta = 0.3$ ,  $Ec = 0.1$ ,  $Pr = 0.4$ ,  $\alpha = 0.2$ ,  $K = 0.2$ ,  $R_T = 0.2$ ,  $Sc = 0.5$ ,  $\xi = 0.1$ ,  $\chi = 0.2$ ,  $A = 0.1$ ,  $B = 0.5$ ,  $\epsilon = 0.3$ ,  $\lambda_1 = 0.1$  and  $\lambda_2 = 0.2$ .

**Table 1** The numerical benchmark for solution convergence at different order of approximations.

Order of Approximation	$H'(0)$	$\theta'(0)$	$\phi'(0)$
7	9.98428	-1.52846	-1.63187
8	9.98438	-1.52876	-1.63220
9	9.98450	-1.52806	-1.63252
10	9.98461	-1.52608	-1.63285
11	9.98472	-1.52665	-1.63318
12	9.98447	-1.52608	-1.63351
15	9.98447	-1.52608	-1.63351
18	9.98447	-1.52608	-1.63351
25	9.98447	-1.52608	-1.63351

**Table 2** The comparative analysis of  $H(\eta)$  and  $H'(\eta)$  for different values of  $\eta$  when  $\gamma = 0.5$  and  $R = 5$  (for Newtonian case).

$\eta$	Gorder et al. [42]		Present result (HAM)	
	$H(\eta)$	$H'(\eta)$	$H(\eta)$	$H'(\eta)$
0.0	0.000	-2.00	0.000	-2.00
0.2	-0.224	-0.360	-0.224	-0.360
0.4	-0.192	0.560	-0.192	0.560
0.6	-0.048	0.760	-0.048	0.760
0.8	0.064	0.240	0.064	0.240
1.0	0.000	-1.00	0.000	-1.000

$$\theta'(0) = -A \exp\left(\frac{-1}{\epsilon(1 + \epsilon\theta(0))}\right), \theta(1) = -R_T, \quad (13)$$

$$\varphi'(0) = B\varphi(0) \exp\left(\frac{-1}{\epsilon(1 + \epsilon\theta(0))}\right), \varphi(1) = \frac{1}{2}.$$

The dimensionless parameters in above equation are stretching rate constant  $\gamma$ , local Grashoff number  $G_r$  [39,40], Frank-Kamenetskii number  $K$ , Hartmann number  $M$ , constant temperature parameter  $R_T$ , Archimedes number  $A_r$ , activation energy parameter  $\epsilon$ , distance  $\delta$ , Schmidt number  $Sc$  and chemical reaction parameter  $\xi$  which are define via following relations:

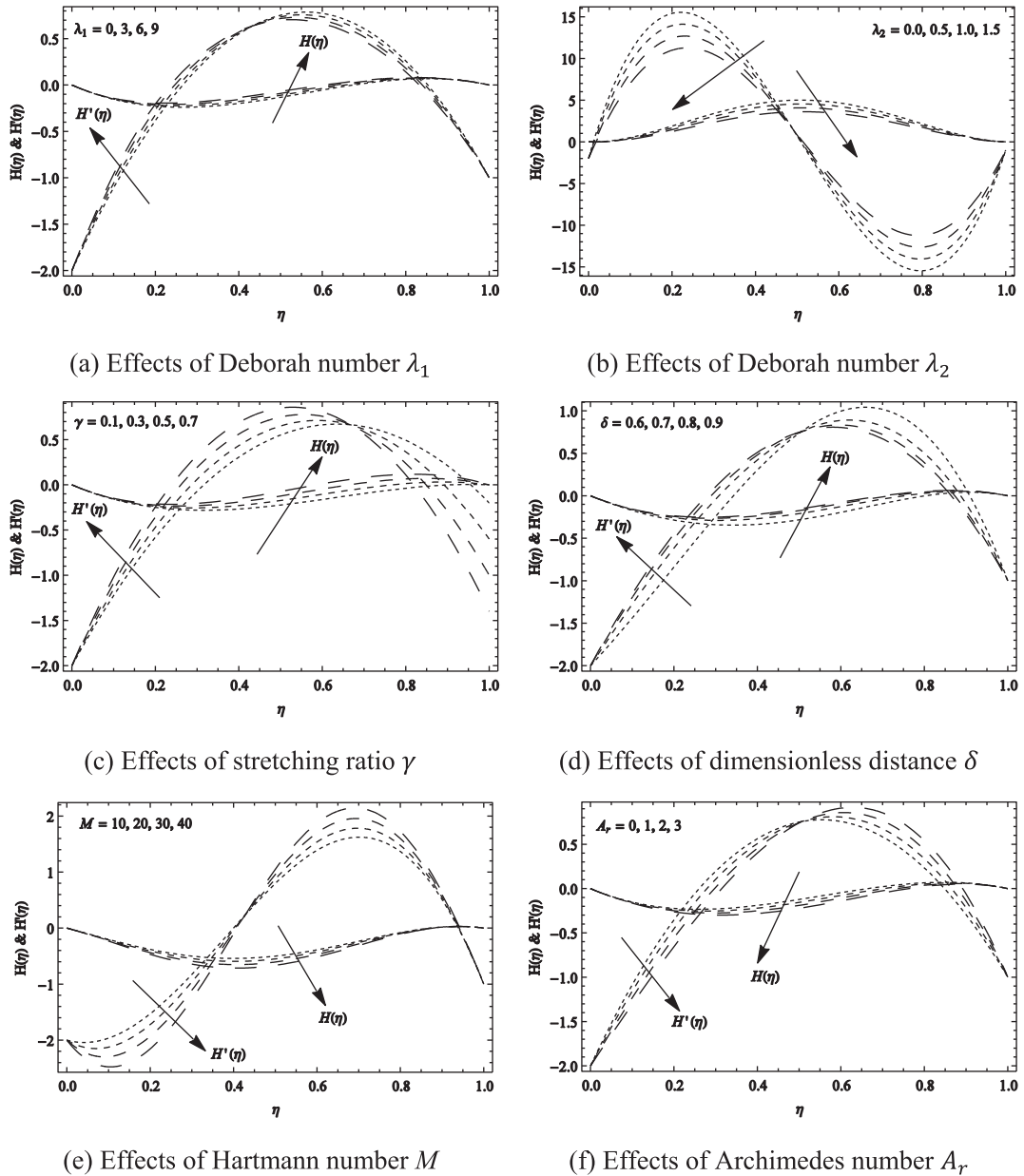


**Fig. 2** Graphs of  $r$  and  $z$  components of velocity (i.e. $H'(\eta)$ & $H(\eta)$  respectively) for  $\gamma = 0.5, h_H = h_\theta = -0.2, M = 0.3, Ec = 1, Pr = 1, R = 5, \delta = 0.5, \epsilon = 0.5, A_r = 20, K = 0.5, A = 3.5, \lambda_1 = 0.5, \lambda_2 = 0.5$  and  $R_T = 2$ .

$$\begin{aligned} \gamma &= \frac{c}{a}, R = \frac{ad^2}{v}, Pr = \frac{\mu c_p}{k}, \delta = \frac{r}{d}, Ec \\ &= \frac{ad^2}{C_p T_0}, K = \frac{Q k_0 a_0 d^2}{K_T T_0 \epsilon} e^{-\frac{1}{\epsilon}}, G_r = \frac{g \beta T_0 r^3}{v^2} \\ \epsilon &= \frac{R_1 T_0}{E}, R_T = \frac{T_1 - T_0}{\epsilon T_0}, A_r = \frac{G_r}{R^2}, M = \frac{\sigma B_0^2}{a \rho}, A \\ &= \frac{Q k_0 C_0 d}{K_T} \frac{E}{R_1 T_0^2}, B = \frac{k_0 d}{D}, \\ \xi &= \frac{k d^2}{v}, \chi = \frac{k C_0 d^2}{(C_2 - C_1)v} \end{aligned}$$

An approximation in Eq. (9) used with assumption of  $(RT_0/E) \ll 1$ . Differentiation of Eq. (9) with respect to similarity variable result following equation

$$\begin{aligned} H^{(iv)} - RHH''' &+ \lambda_1 R(-HH'' - H^2 H^{(iv)} + HH''^2 + H^2 H') \\ &+ \lambda_2 (-2H'' H''' + H'H^{(iv)} + HH^{(v)}) \\ &+ MR[H'' + \lambda_1(H'H'' + HH''')] \\ &+ \frac{RA_r \epsilon}{\delta^4} [2\theta' + \lambda_1(3H'\theta' + 2H\theta'' + H''\theta)] \\ &= 0. \end{aligned} \quad (14)$$

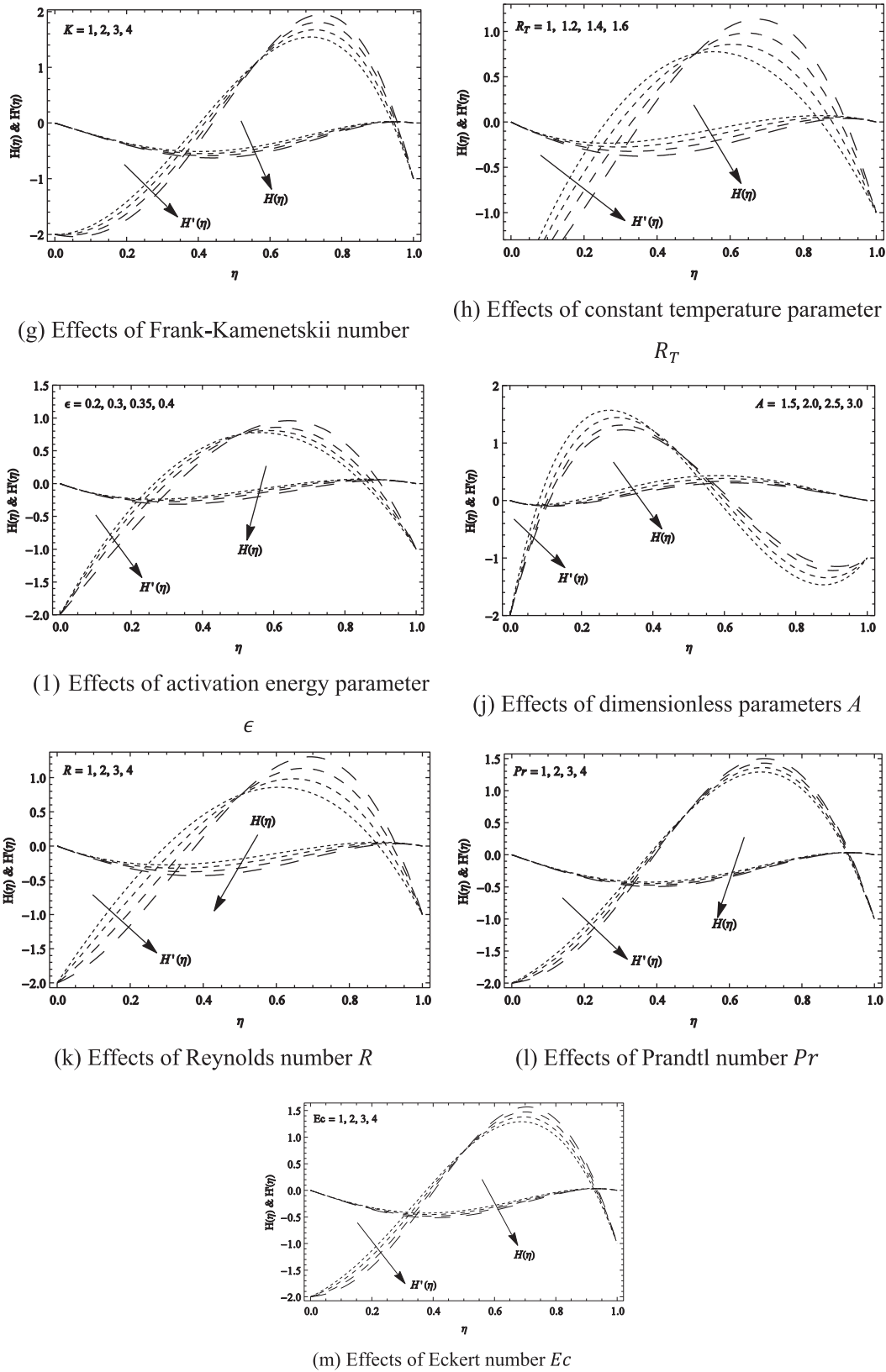
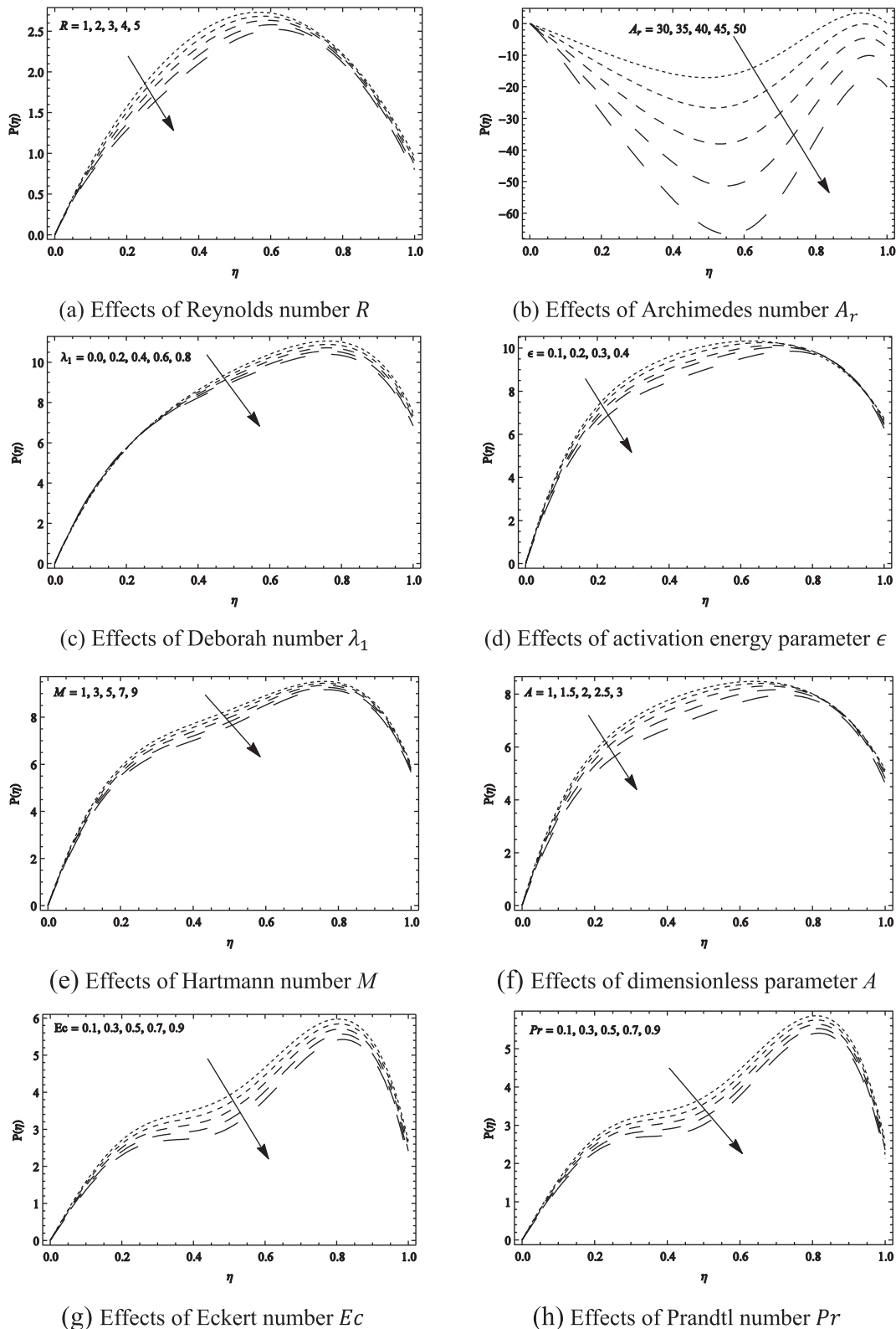
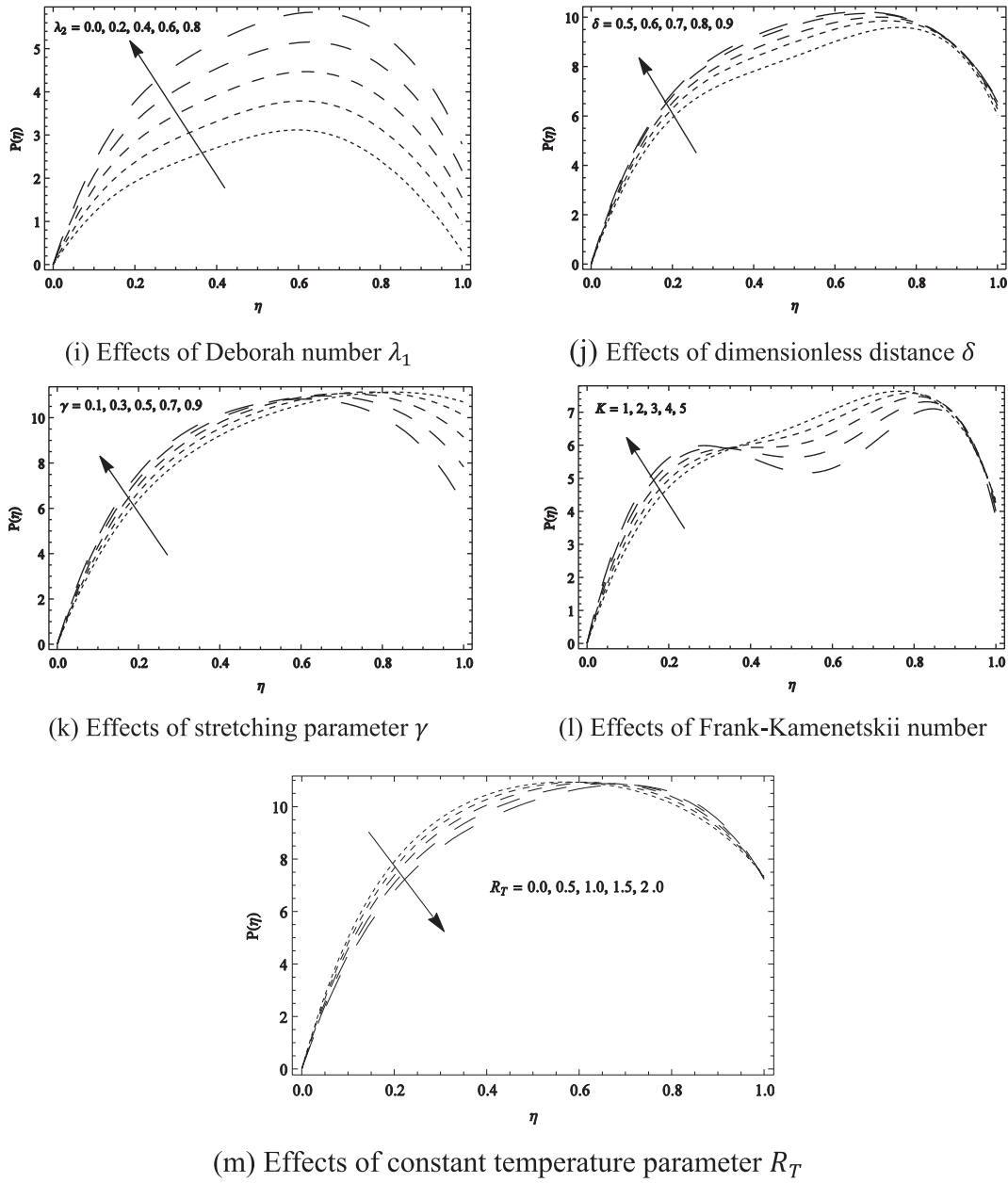


Fig. 2 (continued)



**Fig. 3** Graphs of pressure distribution,  $r$  and  $z$  components of velocity ( $H(\eta)$  &  $H^{\prime}(\eta)$ ) with  $\gamma = 0.5$ ,  $h_H = h_{\theta} = -0.2$ ,  $M = 0.3$ ,  $Ec = 1$ ,  $Pr = 1$ ,  $\alpha = 0.9$ ,  $R = 5$ ,  $\delta = 1.5$ ,  $\epsilon = 0.5$ ,  $A_r = 20$ ,  $K = 0.5$ ,  $A = 3.5$ ,  $\lambda_1 = 0.5$ ,  $\lambda_2 = 1.5$  and  $R_T = 2$ .

**Fig. 3 (continued)**

where  $\lambda_1 = \lambda_1' a$  and  $\lambda_2 = \lambda_2' a$  are the Deborah number in terms of relaxation and retardation respectively.

The non-dimensional expressions of coefficients of skin-friction at lower and upper disk are [40]

$$\left. \begin{aligned} C_{1f} &= \frac{\tau_w}{\frac{1}{2}\rho(\delta r)^2} = -R^{-1}H''(0), \\ C_{2f} &= \frac{\tau_w}{\frac{1}{2}\rho(\delta r)^2} = -R^{-1}H''(1) \end{aligned} \right\} \quad (15)$$

The rate of heat transfer at surface of lower and upper disks is define as [39,40]:

$$N_{1u} = \frac{dq_w}{K_T(T_2 - T_1)} = -\frac{dK_T \frac{\partial T}{\partial z}|_{z=0}}{K_T(T_2 - T_1)} = -\theta'(0), \quad (16)$$

$$N_{2u} = \frac{dq_w}{K_T(T_2 - T_1)} = -\frac{dK_T \frac{\partial T}{\partial z}|_{z=d}}{K_T(T_2 - T_1)} = -\theta'(1). \quad (17)$$

Similarly, the dimensionless form of local Sherwood number is

$$Sh_{1u} = -\varphi(0), \quad (18)$$

$$Sh_{2u} = -\varphi(1), \quad (19)$$

### 3. Solution methodology

The homotopic scheme is used to execute the solutions of governing mathematical expressions. Since this method is quite

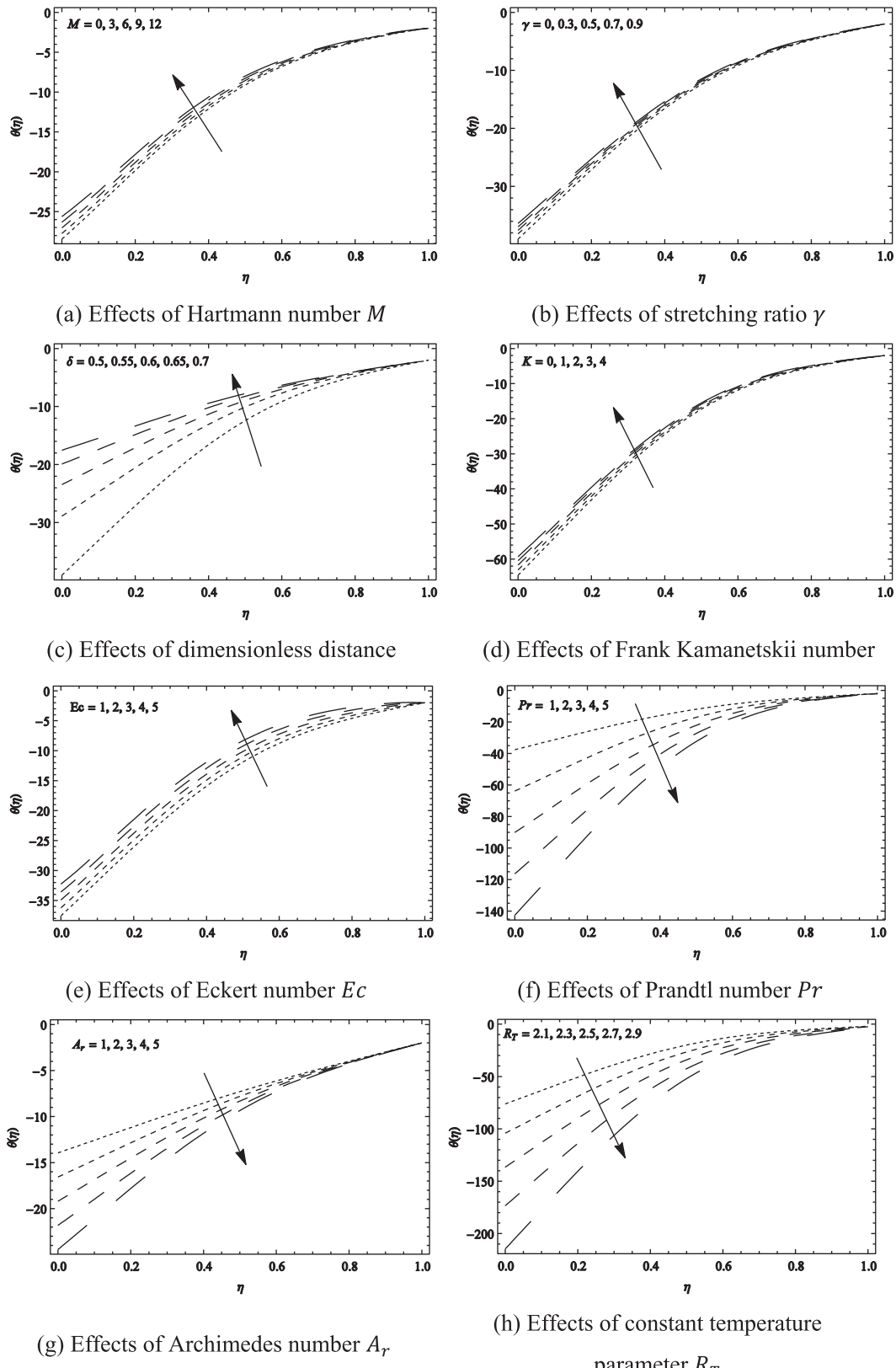


**Fig. 4** Graphs of temperature distribution for  $R = 5, \gamma = 0.5, \hbar_H = \hbar_0 = -0.2, M = 0.3, Ec = 1, Pr = 1, \delta = 0.5, \epsilon = 2, A_r = 20, K = 0.5, A = 1.5, \lambda_1 = 0.5, \lambda_2 = 0.5$  and  $R_T = 2$ .

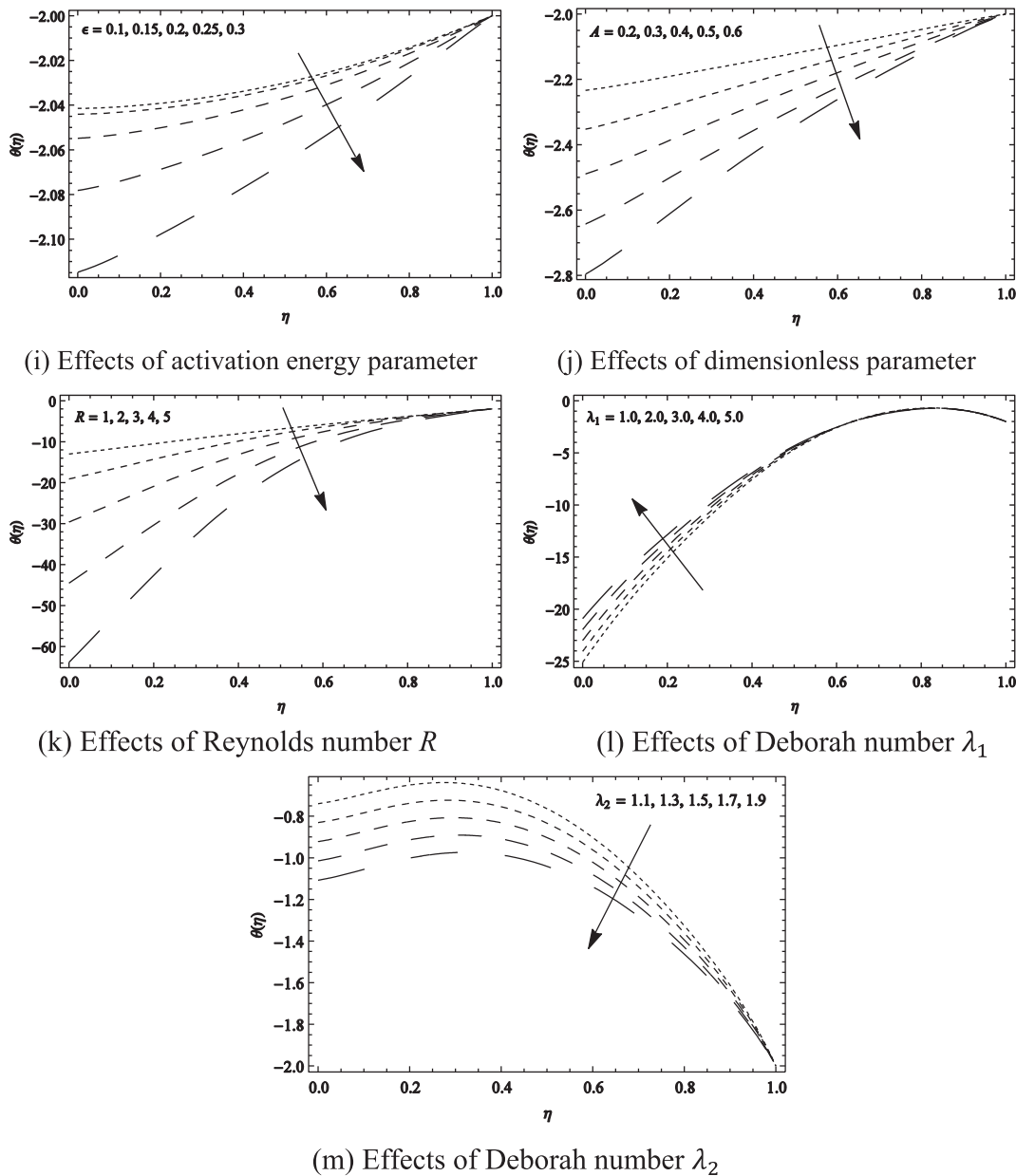


Fig. 4 (continued)

familiar therefore the detail of this analytical scheme is not presented here [39,40].

#### 4. Convergence analysis

Since the homotopic scheme involves the auxiliary parameters  $\bar{h}_H$ ,  $\bar{h}_\theta$  and  $\bar{h}_\phi$  that have key role for the development of convergent solutions. To obtain the possible values of  $\bar{h}_H$ ,  $\bar{h}_\theta$  and  $\bar{h}_\phi$ , the  $\bar{h}$ -curves at fifteen order of approximations are designed in Fig. 1. From this curve, it is noted that the possible ranges of auxiliary parameters are  $-1.2 \leq \bar{h}_H \leq 0.1$ ,  $-1.1 \leq \bar{h}_\theta \leq 0.1$  and  $-0.9 \leq \bar{h}_\phi \leq 0.1$ . For best convergence, the appropriate values of  $\bar{h}_H$ ,  $\bar{h}_\theta$  and  $\bar{h}_\phi$  are  $\bar{h}_H = \bar{h}_\theta = \bar{h}_\phi = -0.2$ . Table 1 aim to examine the convergence of obtained solution at various approximations. The conver-

gence for all profiles is achieved at 12th order of approximations. Table 2 indicates the comparison of simulated solution with work of Gorder et al. [42]. The obtained results showed an excellent agreement.

#### 5. Discussion

The physical assessment of involved flow parameters like Deborah number for relaxation time  $\lambda_1$ , Deborah number for retardation time  $\lambda_2$ , Reynolds number  $R$ , stretching ratio  $\gamma$ , Prandtl number  $Pr$ , Eckert number  $Ec$ , Frank-Kamenetskii number  $K$ , parameter of activation energy  $\epsilon$ , parameter of constant temperature  $R_T$ , Hartmann number  $M$ , Archimedes number  $A_r$ , dimensionless distance  $\delta$ , chemical reaction parameter  $\xi$ , non dimensional parameters  $A, B, \chi$  and Schmidt number

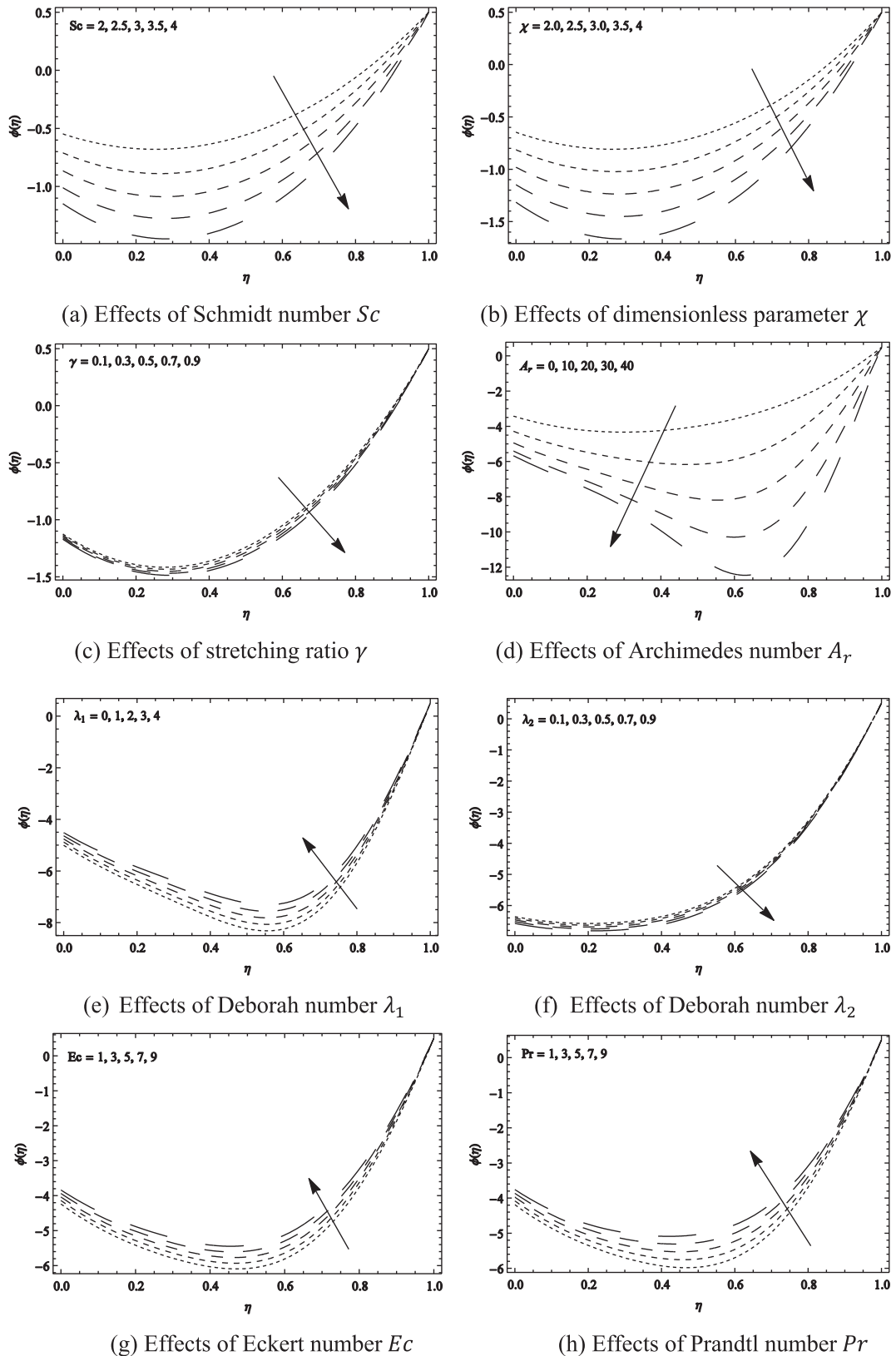


**Fig. 5** Graphs of concentration distribution for  $R = 5; \gamma = 0.5, h_H = h_\theta = h_\phi = -0.2, M = 1, Ec = 1, Pr = 1, \alpha = 0.9, \delta = 1.5, \epsilon = 2, A_r = 200, K = 0.5, A = 3.5, B = 3, Sc = 4, \chi = 3.5, \xi = 3, \lambda_1 = 0.5, \lambda_2 = 1.5$  and  $R_T = 2$ .

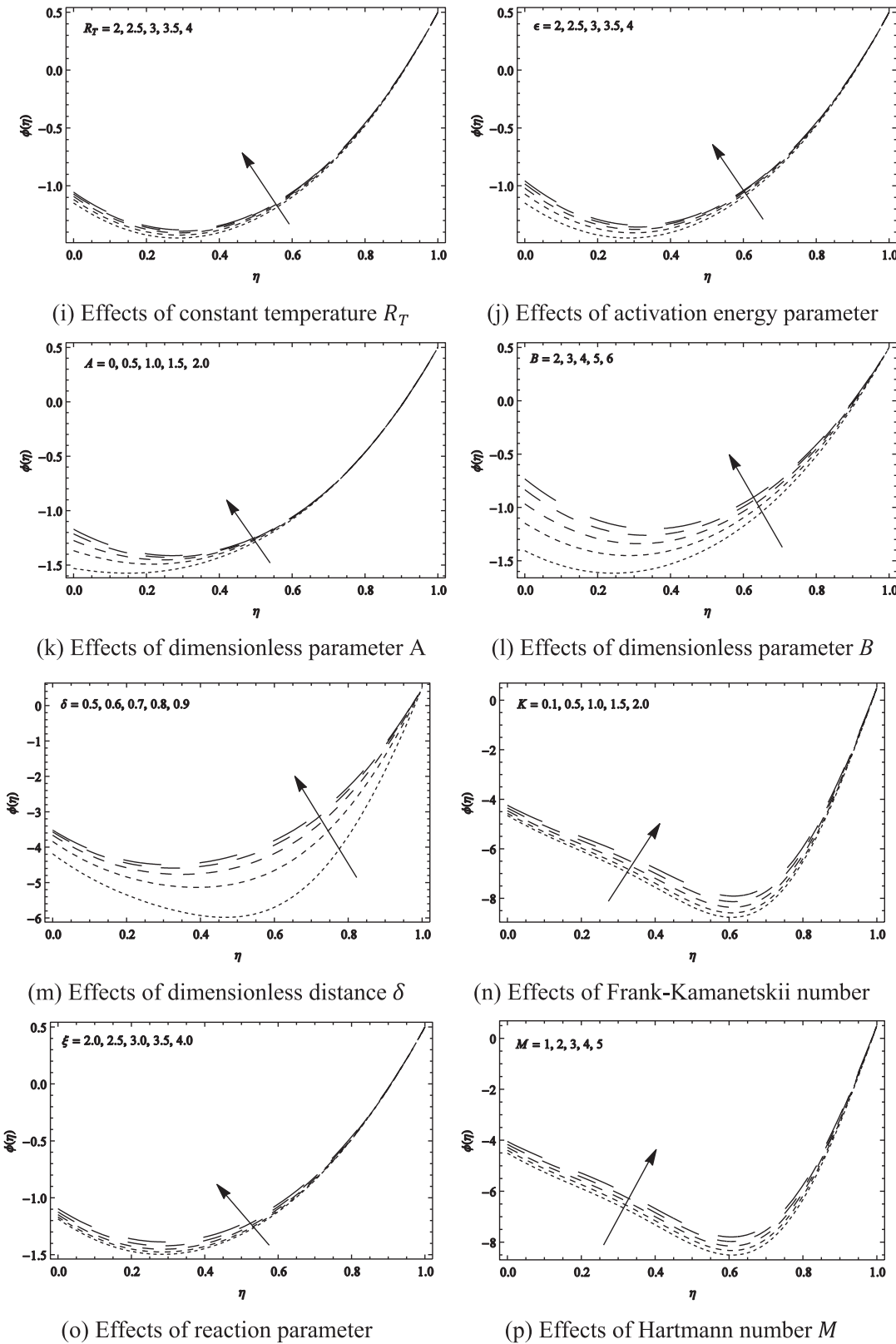


Fig. 5 (continued)

**Table 3** Analysis for coefficients of skin-friction for different parameters at both disks.

$\Gamma$	$M$	$R$	$Pr$	$Ec$	$\delta$	$\epsilon$	$A_r$	$R_T$	$K$	$A$	$\lambda_1$	$\lambda_2$	lower disk	upper disk
0.2	0.3	05	01	01	0.5	0.5	02	02	0.5	3.5	0.5	0.5	13.6360	-15.3875
0.4	0.3	05	01	01	0.5	0.5	02	02	0.5	3.5	0.5	0.5	15.2908	-18.5411
0.6	0.3	05	01	01	0.5	0.5	02	02	0.5	3.5	0.5	0.5	16.9335	-21.7165
0.5	03	05	01	01	0.5	0.5	02	02	0.5	3.5	0.5	0.5	15.0460	-19.8463
0.5	06	05	01	01	0.5	0.5	02	02	0.5	3.5	0.5	0.5	13.8416	-19.5440
0.5	09	05	01	01	0.5	0.5	02	02	0.5	3.5	0.5	0.5	12.6186	-19.2503
0.5	0.3	1.0	01	01	0.5	0.5	02	02	0.5	3.5	0.5	0.5	17.6862	-18.4657
0.5	0.3	2.0	01	01	0.5	0.5	02	02	0.5	3.5	0.5	0.5	16.9031	-19.2941
0.5	0.3	3.0	01	01	0.5	0.5	02	02	0.5	3.5	0.5	0.5	16.1141	-20.1257
0.5	0.3	05	01	01	0.5	0.5	02	02	0.5	3.5	0.5	0.5	5.45294	-31.0109
0.5	0.3	05	02	01	0.5	0.5	02	02	0.5	3.5	0.5	0.5	4.10354	-32.0518
0.5	0.3	05	03	01	0.5	0.5	02	02	0.5	3.5	0.5	0.5	2.75415	-33.0927
0.5	0.3	05	01	01	0.5	0.5	02	02	0.5	3.5	0.5	0.5	5.45294	-31.0109
0.5	0.3	05	01	02	0.5	0.5	02	02	0.5	3.5	0.5	0.5	4.02330	-32.9072
0.5	0.3	05	01	03	0.5	0.5	02	02	0.5	3.5	0.5	0.5	2.59367	-34.8034
0.5	0.3	05	01	01	1.2	0.5	02	02	0.5	3.5	0.5	0.5	19.9483	-15.9952
0.5	0.3	05	01	01	1.3	0.5	02	02	0.5	3.5	0.5	0.5	19.9810	-15.9601
0.5	0.3	05	01	01	1.4	0.5	02	02	0.5	3.5	0.5	0.5	20.0032	-15.9361
0.5	0.3	05	01	01	0.5	0.1	02	02	0.5	3.5	0.5	0.5	20.0620	-15.9043
0.5	0.3	05	01	01	0.5	0.2	02	02	0.5	3.5	0.5	0.5	20.0149	-15.9847
0.5	0.3	05	01	01	0.5	0.3	02	02	0.5	3.5	0.5	0.5	19.6796	-16.3627
0.5	0.3	05	01	01	0.5	0.5	01	02	0.5	3.5	0.5	0.5	18.0908	-17.9963
0.5	0.3	05	01	01	0.5	0.5	02	02	0.5	3.5	0.5	0.5	16.1141	-20.1257
0.5	0.3	05	01	01	0.5	0.5	03	02	0.5	3.5	0.5	0.5	14.1375	-22.2551
0.5	0.3	05	01	01	0.5	0.5	02	0.5	0.5	3.5	0.5	0.5	22.0442	-13.7375
0.5	0.3	05	01	01	0.5	0.5	02	0.6	0.5	3.5	0.5	0.5	21.2535	-14.5892
0.5	0.3	05	01	01	0.5	0.5	02	0.7	0.5	3.5	0.5	0.5	20.4628	-15.4410
0.5	0.3	05	01	01	0.5	0.9	02	02	0.1	3.5	0.5	0.5	16.0255	-20.5039
0.5	0.3	05	01	01	0.5	0.9	02	02	0.2	3.5	0.5	0.5	15.8482	-21.2604
0.5	0.3	05	01	01	0.5	0.9	02	02	0.3	3.5	0.5	0.5	15.6709	-22.0169
0.5	0.3	05	01	01	0.5	0.9	02	02	0.5	1.5	0.5	0.5	18.9301	-17.2047
0.5	0.3	05	01	01	0.5	0.9	02	02	0.5	2.0	0.5	0.5	18.4223	-17.7313
0.5	0.3	05	01	01	0.5	0.9	02	02	0.5	2.5	0.5	0.5	17.8104	-18.3658
0.5	0.3	05	01	01	0.5	0.9	02	02	0.5	0.5	0.1	0.5	16.4531	-20.0869
0.5	0.3	05	01	01	0.5	0.9	02	02	0.5	0.5	0.2	0.5	17.1309	-20.0095
0.5	0.3	05	01	01	0.5	0.9	02	02	0.5	0.5	0.3	0.5	17.8087	-19.9320
0.5	0.3	05	01	01	0.5	0.9	02	02	0.5	0.5	0.5	0.1	16.6555	-19.644
0.5	0.3	05	01	01	0.5	0.9	02	02	0.5	0.5	0.5	0.2	17.7381	-18.6807
0.5	0.3	05	01	01	0.5	0.9	02	02	0.5	0.5	0.5	0.3	18.8207	-17.7175

$Sc$  on radial velocity(i.e.  $H'(\eta)$ ) and axial directions (i.e.  $H(\eta)$ ), pressure, temperature and concentration distribution with help of Figs. (2-5).

Fig. 2(a-d) elaborates the importance of relaxation time Deborah number, retardation time Deborah number, dimensionless distance and stretching ratio on  $r$  and  $z$  components of velocity. Fig. 2(a) shows that the  $z$  component of liquid velocity is enhanced for both Deborah numbers ( $\lambda_1, \lambda_2$ ). Physically, Deborah number  $\lambda_1$  has direct relation to relaxation time so longer relaxation time results more dominant elastic effects associated with Oldroyd-B fluid which cause an increase in velocity. The  $r$  component of velocity enhances for certain height of disks and then reduces for the values of relaxation time Deborah number. Fig. 2(b) shows the impact of Deborah number of retardation time  $\lambda_2$  on radial velocity and axial velocity where quite reverse observations are observed. The radial velocity is increasing function of stretching ratio and dimensionless distance while axial velocity raise up to certain height of disks channel and then started decreasing

(Fig. 2(c)-2(d)). Fig. 2(e) illustrates the impact of Hartmann number on radial component of velocity. It is observed that radial velocity reduces as the values of Hartmann number increases because a drag force is appeared due to Lorentz force which create a resistance to liquid flow. The axial velocity decreases up to certain vertical distance between the disks and then starts increasing as value of Hartmann varies. Fig. 2(f)-2(m) elucidate the influence of  $A_r, K, R_T, \epsilon, A, R, Ec$  and  $Pr$  on axial and radial velocity. The effects of these parameters are similar to Hartmann number. Physically, Archimedes number reflects the ratio of gravitational to viscous force. The dimensionless number enables to determine the fluid particles movement due to density differences.

The comparison of Fig. 3(a)-3(h) with Fig. 3(i)-3(j) demonstrate that pressure is decreasing function of  $R, A_r, \lambda_1, \epsilon, M, A, Ec$  and  $Pr$ . On other hand, the effects of Deborah number of retardation time and distance constant are opposite to that of  $R, A_r, \lambda_1, \epsilon, M, A, Ec$  and  $Pr$ . From Fig. 3(k)-3(l), it is found that as value of stretching ratio and Frank-Kamenetskii

**Table 4** The Nusselt number values at lower and upper disks.

$\gamma$	$M$	$R$	$Pr$	$Ec$	$\delta$	$\epsilon$	$A_r$	$R_T$	$K$	$A$	$\lambda_1$	$\lambda_2$	lower disk	upper disk
0.3	0.3	05	01	01	03	02	20	02	0.5	1.5	0.5	0.5	-106.423	-13.3177
0.6	0.3	05	01	01	03	02	20	02	0.5	1.5	0.5	0.5	-103.143	-11.6023
0.9	0.3	05	01	01	03	02	20	02	0.5	1.5	0.5	0.5	-99.8634	-9.88681
0.5	0.1	05	01	01	03	02	20	02	0.5	1.5	0.5	0.5	-104.324	-12.2064
0.5	0.2	05	01	01	03	02	20	02	0.5	1.5	0.5	0.5	-104.280	-12.1903
0.5	0.3	05	01	01	03	02	20	02	0.5	1.5	0.5	0.5	-104.237	-12.1741
0.5	0.3	01	01	01	03	02	20	02	0.5	1.5	0.5	0.5	-11.7541	-8.28170
0.5	0.3	02	01	01	03	02	20	02	0.5	1.5	0.5	0.5	-22.8453	-8.57386
0.5	0.3	03	01	01	03	02	20	02	0.5	1.5	0.5	0.5	-41.9561	-8.78831
0.5	0.3	05	0.5	01	03	02	20	02	0.5	1.5	0.5	0.5	-56.4597	-10.9130
0.5	0.3	05	1.0	01	03	02	20	02	0.5	1.5	0.5	0.5	-104.237	-12.1741
0.5	0.3	05	1.5	01	03	02	20	02	0.5	1.5	0.5	0.5	-152.014	-13.4352
0.5	0.3	05	01	0.5	03	02	20	02	0.5	1.5	0.5	0.5	-8.50626	-9.53212
0.5	0.3	05	01	1.0	03	02	20	02	0.5	1.5	0.5	0.5	-8.37789	-9.40389
0.5	0.3	05	01	1.5	03	02	20	02	0.5	1.5	0.5	0.5	-8.24952	-9.27566
0.5	0.3	05	01	01	1.0	02	20	02	0.5	1.5	0.5	0.5	-12.9525	-8.12087
0.5	0.3	05	01	01	1.3	02	20	02	0.5	1.5	0.5	0.5	-9.62955	-8.57133
0.5	0.3	05	01	01	1.6	02	20	02	0.5	1.5	0.5	0.5	-8.79385	-8.88103
0.5	0.3	05	01	01	03	0.2	20	02	0.5	1.5	0.5	0.5	-0.01029	-0.09124
0.5	0.3	05	01	01	03	0.3	20	02	0.5	1.5	0.5	0.5	-0.05737	-0.13709
0.5	0.3	05	01	01	03	0.4	20	02	0.5	1.5	0.5	0.5	-0.14377	-0.21925
0.5	0.3	05	01	01	03	02	10	02	0.5	1.5	0.5	0.5	-56.4612	-10.9133
0.5	0.3	05	01	01	03	02	15	02	0.5	1.5	0.5	0.5	-80.3490	-11.5437
0.5	0.3	05	01	01	03	02	20	02	0.5	1.5	0.5	0.5	-104.237	-12.1741
0.5	0.3	05	01	01	03	02	20	1.1	0.5	1.5	0.5	0.5	-1.48980	-0.33151
0.5	0.3	05	01	01	03	02	20	1.4	0.5	1.5	0.5	0.5	-17.6711	-2.48767
0.5	0.3	05	01	01	03	02	20	1.7	0.5	1.5	0.5	0.5	-51.9201	-6.43519
0.5	0.3	05	01	01	03	02	20	02	0.1	1.5	0.5	0.5	-102.891	-11.7608
0.5	0.3	05	01	01	03	02	20	02	0.2	1.5	0.5	0.5	-100.374	-10.9970
0.5	0.3	05	01	01	03	02	20	02	0.3	1.5	0.5	0.5	-98.0890	-10.3167
0.5	0.3	05	01	01	03	02	20	02	0.5	1.5	0.5	0.5	-21.4106	6.36069
0.5	0.3	05	01	01	03	02	20	02	0.5	2.0	0.5	0.5	-6.55988	3.84972
0.5	0.3	05	01	01	03	02	20	02	0.5	2.5	0.5	0.5	-3.17108	2.92798
0.5	0.3	05	01	01	03	02	20	02	0.5	1.5	0.1	0.5	-124.646	55.7710
0.5	0.3	05	01	01	03	02	20	02	0.5	1.5	0.2	0.5	-123.478	55.7486
0.5	0.3	05	01	01	03	02	20	02	0.5	1.5	0.3	0.5	-122.311	55.7262
0.5	0.3	05	01	01	03	02	20	02	0.5	1.5	0.5	0.1	-110.573	50.4592
0.5	0.3	05	01	01	03	02	20	02	0.5	1.5	0.5	0.2	-81.9662	39.8299
0.5	0.3	05	01	01	03	02	20	02	0.5	1.5	0.5	0.3	-54.3004	29.2230

number vary, a rise in pressure up to certain height of disk is noticed which later on decrease gradually. Fig. 3(m) demonstrates that behavior of constant temperature parameter is opposite to that of stretching ratio and Frank-Kamanetskii number.

From Fig. 4(a), it is revealed that temperature  $\theta$  increases as the value of Hartmann number increase. For better engineering and industrial final products the variation of applied magnetic field play a fascinating role. The fluid temperature is an increasing function of stretching ratio, dimensionless distance and Frank-Kamanetskii number as shown in Fig. 4(b)-4(d). The ratio of kinetic energy to enthalpy is known as Eckert number which means that kinetic energy of fluid particle increases for higher values of Eckert number and subsequently a progressive temperature profile is noted (Fig. 4(e)). It is observed from Fig. 4(f) that fluid temperature is a decreasing function of Prandtl number  $r$ . Physically, increasing values of Prandtl number lead to lower thermal diffusivity. This weaker thermal diffusivity causes a reduction in fluid temperature. Fig. 4(g)-4(k) demonstrate that dimensionless

temperature  $\theta$  is an increasing function of  $A_r$ ,  $R_T$ ,  $\epsilon$ ,  $A$  and  $R$ . Fig. 4(i) reflects that upon increasing Deborah number of relaxation time  $\lambda_1$ , the fluid temperature enhanced. It is due to the fact that higher relaxation time leads to increment in temperature. On the other hand, fluid temperature is decreasing function of Deborah number of retardation time  $\lambda_2$ . The higher retardation time causes a reduction in fluid temperature and presented in Fig. 4(m).

Fig. 5(a) aims to examine the change in concentration profile  $\varphi$  for various values of Schmidt number  $Sc$ . It is evident from this figure that concentration field  $\varphi$  decreases as the value of Schmidt number increases. Since Schmidt number is the ratio of momentum diffusivity to mass diffusivity. Therefore, Schmidt number depends on molecular diffusivity and higher value of Schmidt number causes a lower molecular diffusivity. Fig. 5-(b)-(d) reveal that concentration profile is a decreasing function of  $\chi$ ,  $\gamma$ , and  $A_r$ . It is noticed from Fig. 5(e)-5(f) that  $\lambda_1$  causes an enhancement in concentration field while reverse trend is noted for  $\lambda_2$ . Fig. 5(g)-5(h) indicate that the concentration field

**Table 5** The change in Sherwood number at lower and upper disks.

$\gamma$	$M$	$R$	$A$	$B$	$\delta$	$A_r$	$\epsilon$	$R_T$	$\chi$	$\xi$	lower disk	upper disk
0.3	0.3	05	3.5	03	0.5	20	02	02	3.5	03	2.10579	-5.78484
0.6	0.3	05	3.5	03	0.5	20	02	02	3.5	03	2.13697	-5.94809
0.9	0.3	05	3.5	03	0.5	20	02	02	3.5	03	2.16815	-6.11134
0.5	01	05	3.5	03	0.5	20	02	02	3.5	03	8.28998	-33.1546
0.5	02	05	3.5	03	0.5	20	02	02	3.5	03	8.21310	-32.8643
0.5	03	05	3.5	03	0.5	20	02	02	3.5	03	8.13664	-32.5752
0.5	0.3	01	3.5	03	0.5	20	02	02	3.5	03	2.08664	-5.80575
0.5	0.3	02	3.5	03	0.5	20	02	02	3.5	03	2.09663	-5.82773
0.5	0.3	03	3.5	03	0.5	20	02	02	3.5	03	2.10661	-5.84971
0.5	0.3	05	1.0	03	0.5	20	02	02	3.5	03	1.56751	-5.92949
0.5	0.3	05	1.5	03	0.5	20	02	02	3.5	03	1.75776	-5.91730
0.5	0.3	05	2.0	03	0.5	20	02	02	3.5	03	1.89123	-5.90875
0.5	0.3	05	3.5	2.0	0.5	20	02	02	3.5	03	1.10392	-6.36570
0.5	0.3	05	3.5	2.3	0.5	20	02	02	3.5	03	1.46210	-6.22233
0.5	0.3	05	3.5	2.6	0.5	20	02	02	3.5	03	1.73686	-6.09512
0.5	0.3	05	3.5	03	1.0	20	02	02	3.5	03	6.48628	-17.9236
0.5	0.3	05	3.5	03	1.5	20	02	02	3.5	03	6.32064	-17.0654
0.5	0.3	05	3.5	03	2.0	20	02	02	3.5	03	6.29198	-16.9202
0.5	0.3	05	3.5	03	0.5	10	02	02	3.5	03	7.65348	-25.2967
0.5	0.3	05	3.5	03	0.5	20	02	02	3.5	03	8.34404	-33.3586
0.5	0.3	05	3.5	03	0.5	30	02	02	3.5	03	8.35031	-41.0384
0.5	0.3	05	3.5	03	0.5	20	1.0	02	3.5	03	1.42007	-6.14956
0.5	0.3	05	3.5	03	0.5	20	1.5	02	3.5	03	1.90190	-5.98219
0.5	0.3	05	3.5	03	0.5	20	2.0	02	3.5	03	2.12658	-5.89367
0.5	0.3	05	3.5	03	0.5	20	02	10	3.5	03	1.85666	-5.91096
0.5	0.3	05	3.5	03	0.5	20	02	20	3.5	03	1.82885	-5.91275
0.5	0.3	05	3.5	03	0.5	20	02	30	3.5	03	1.81982	-5.91332
0.5	0.3	05	3.5	03	0.5	20	02	02	02	03	1.21470	-3.89184
0.5	0.3	05	3.5	03	0.5	20	02	02	03	03	1.82262	-5.22640
0.5	0.3	05	3.5	03	0.5	20	02	02	04	03	2.43053	-6.56095
0.5	0.3	05	3.5	03	0.5	20	02	02	3.5	3.0	2.12658	-5.89367
0.5	0.3	05	3.5	03	0.5	20	02	02	3.5	3.4	2.09178	-5.88951
0.5	0.3	05	3.5	03	0.5	20	02	02	3.5	3.8	2.05284	-5.87825

enhanced as the values of Prandtl number and Eckert number increases. The concentration field is an increasing function of  $R_T, \epsilon, A, B, \delta$  and  $K$  and shown in Fig. 5(i)-5(n). It is evident from Fig. 5(o) that chemical reaction rate parameter increases the concentration distribution  $\varphi$ . Fig. 5(p) shows that concentration profile get larger with Hartmann number variation.

Table 3 represents the variation of skin friction coefficient at upper disk surface  $RC_{1f}$  and lower surface  $RC_{2f}$ . The progressive numerical values at upper disk surface are noted for all parameters. An increasing variation at upper surface of disk is noticed with  $\Gamma, \delta, \lambda_1$  and  $\lambda_2$ . Table 4 examines the effects of  $\gamma, M, \lambda_1, \lambda_2, R, Pr, Ec, \delta, \epsilon, A_r, R_T, A$  and  $K$  on Nusselt number  $N_{1u}$  (upper surface) and  $N_{2u}$  (lower surface). The heat transfer at upper surface is more dominant as compared to lower disk surface. The heat transfer rate enhanced with  $Pr, A_r$  while opposite trend has been noticed upon increasing  $\lambda_1$  and  $\lambda_2$ . The effects of different parameters on Sherwood number are displayed in Table 5. The higher concentration is observed associated with  $\gamma, R$  and  $\chi$  at both disks surfaces.

## 6. Conclusions

In this analysis, combined heat and mass transfer assessment in flow of Oldroyd-B induced has been examined in presence of Joule heating, chemical reaction and Ohmic dissipations. The flow has been induced by radially moving isothermally

and exothermally stretching disks. The important observations claimed from this work are listed below:

- The skin friction coefficient decreases when Reynolds number, Prandtl number, Eckert number, Archimedes number, parameter of constant temperature and dimensionless distance parameter increases.
- The tangential stresses are increasing function of stretching ratio up to certain height of disks channel and then start increasing. On the other hand the effect of magnetic parameter on tangential stresses is opposite to that of stretching ratio.
- Upon increment of Deborah numbers and dimensionless distance parameter, the skin friction coefficient at both disks also increases.
- The rate of heat transfer on both disks increases as the value of stretching parameter, Hartmann number, Eckert number and Frank-Kamenetskii number increases. In contrast, the rate of heat transfer on both disks are decreasing function of Prandtl number, activation energy parameter, Archimedes number and constant temperature parameter.
- The rate of heat transfer at lower disk increases and at upper disk decreases when the values of dimensionless distance, Archimedes number and Deborah number increases while the behavior of Reynolds number is opposite to that of dimensionless distance.

- When the values of dimensionless parameter and activation energy parameter increases the rate of mass transfer on both disks increases.
- The behavior of constant temperature on concentration distribution is opposite to that of activation energy constant.

### Declaration of Competing Interest

The authors declare that they have no known competing financial interests or personal relationships that could have appeared to influence the work reported in this paper.

### Acknowledgments

The research was supported by the National Natural Science Foundation of China (Grant Nos. 11971142, 11871202, 61673169, 11701176, 11626101, 11601485).

### References

- [1] T. Hayat, M. Awais, M. Qasim, Awatif A. Hendi, Effects of mass transfer on the stagnation point flow of an upper-conveected Maxwell (UCM) fluid, *International Journal of Heat and Mass Transfer*, 2011, 54: 3777–3782.
- [2] Z. Abbas, M. Sajid, T. Hayat, MHD boundary layer flow of an upper-conveected Maxwell fluid in porous channel, *Theoretical Computational Fluid Dynamics* 20 (2006) 229–238.
- [3] K. Sadeghy, A.H. Najafi, M. Saffaripour, Sakiadis flow of an upper-conveected Maxwell fluid, *Int. J. Non-Linear Mech.* 40 (2005) 1220–1228.
- [4] Z. Abbas, M. Sajid, T. Hayat, MHD boundary-layer flow of an upper-conveected Maxwell fluid in a porous channel, *Theor. Comput. Fluid Dyn.* 20 (2006) 229–238.
- [5] T. Hayat, Z. Abbas, M. Sajid, Series solution for the upper convected Maxwell fluid over a porous stretching plate, *Phys. Lett. A* 358 (2006) 396–403.
- [6] A.A. Pahlavan, V. Aliakbar, F.V. Farahani, K. Sadeghy, MHD flows of UCM fluids above porous stretching sheets using two auxiliary-parameter homotopy analysis method, *Commun. Nonlinear Sci. Numer. Simul.* 14 (2009) 473–488.
- [7] S.A. Shehzad, M. Qasim, T. Hayat, M. Sajid, S. Obaidat Boundary layer flow of Maxwell fluid with power law heat flux and heat source, *Int. J. Numer. Methods HeatFluid Flow*, 23 (2013) 1225–1241.
- [8] T. Hayat, S.A. Shehzad, A. Alsaedi, MHD three-dimensional flow of Maxwell fluid with variable thermal conductivity and heat source/sink, *Int. J. Numer. Methods HeatFluid Flow* 24 (2014) 1073–1085.
- [9] Panchun Liang, Shaowei Wang, Moli Zhao Numerical study of rotating electroosmotic flow of Oldroyd-B fluid in a microchannel with slip boundary condition, *Chinese Journal of Physics* 65 (June 2020) 459–471.
- [10] Muhammad Naveed Khan, Sohail Nadeem, Naeem Ullah, Anber Saleem, Theoretical treatment of radiative Oldroyd-B nanofluid with microorganism pass an exponentially stretching sheet, *Surfaces and Interfaces* 21 (December 2020).
- [11] Nargis Khan, Muhammad Sadiq Hashmi, Sami Ullah Khan, Iskander Tili, Mostafa S. Shadloo and Faryal Chaudhry, Effects of homogeneous and heterogeneous chemical features in Oldroyd-B fluid flow between stretching disks with velocity and temperature boundary assumptions, *Mathematical Problems in Engineering*, volume (2020), Article ID 5284906, 13 pages.
- [12] A. Postelnicu, Onset of convection in a horizontal porous layer driven by catalytic surface reaction on the lower wall, *International Journal of Heat and Mass Transfer* 52 (2009) 2466–2470.
- [13] I. Pop, T. Grosan, R. Cornelia, Effect of heat generated by an exothermic reaction on the fully developed mixed convection flow in a vertical channel, *1 Commun Nonlinear SciNumerSimulat* 15 (2010) 471–474.
- [14] D.B. Ingham, S.D. Harris, I. Pop, Free-convection boundary layers at a threedimensionalstagnation point driven by exothermic surface reaction, *HybridMethods Eng.* 1 (1999) 401–417.
- [15] M.A. Chaudhary, J. Merkin, Free convection stagnation point boundary layersdriven by catalytic surface reactions: I. The steady states, *J. Eng. Math.* 1994, 28: 145–171.
- [16] M.A. Chaudhary, J. Merkin, Free convection stagnation point boundary layers driven by catalytic surface reactions: II. Times to ignition, *J. Eng. Math.* 30 (1996) 403–415.
- [17] J. Merkin, M.A. Chaudhary, Free convection boundary layers on vertical surfaces driven by an exothermic surface reaction, *Quart. J. Appl. Math.* 47 (1994) 405–428.
- [18] M.A. Chaudhary, A. Liffan, J. Merkin, Free convection boundary layers driven byexothermic surface reactions: critical ambient temperature, *Math. Eng. Ind.* 5 (1995) 129–145.
- [19] M.I. Khan, M. Waqas, T. Hayat, A. Alsaedi, A comparative study of Casson fluid with homogeneous-heterogeneous reactions, *J. Colloid Interface Sci.* 498 (2017) 85–90.
- [20] R. Muhammad, M.I. Khan, N.B. Khan, M. Jameel, Magnetohydrodynamics (MHD) radiated nanomaterial viscous material flow by a curved surface with second order slip and entropy generation, *Comput. Meth. Prog. Biomed.* 189 (2020).
- [21] J. Merkin, T. Mahmood, Convective flows on reactive surfaces in porous media, *Transport Porous Media* 47 (1998) 279–293.
- [22] T. Mahmood, J. Merkin, The convective boundary-layer flow on a reactingsurface in a porous medium, *Transport Porous Media* 32 (1999) 285–298.
- [23] B.J. Minto, D.B. Ingham, I. Pop, Free convection driven by an exothermic on avertical surface embedded in porous media, *Int. J. Heat Mass Transfer* 41 (1998) 11–23.
- [24] H.D. Nguyen, S. Paik, R. Douglas, I. Pop, Unsteady non-Darcy reaction-driven flow from an anisotropic cylinder in porous media, *Chemical Eng. Sci.* 51 (1996) 4963–4977.
- [25] S. Srinivas, R. Muthuraj, Effects of thermal radiation and space porosity on MHD mixed convection flow in a vertical channel using homotopy analysis method, *Commun Nonlinear SciNumerSimulat* 15 (2010) 2098–2108.
- [26] G.K. Ramesh, B.J. Gireesha, Influence of heat source/sink on a Maxwell fluid over a stretching surface with convectiveboundary condition in the presence of nanoparticles, *Ain Shams Engineering Journal*, 2014, 5: 991–998.
- [27] A. Postelnicu ,T. Grosan T, I. Pop,The effect of variable viscosity onforced convection flow past a horizontal flat plate in a porousmedium with internal heat generation, *Mech Res Commun*, 2001, 28:331–7.
- [28] M. Abo-EladahabEmad, A. El Aziz Mohamed, Blowing/suction effect on hydromagnetic heat transfer by mixed convection from an inclined continuously stretching surface with internal heat generation/absorption, *Int J ThermSci* 43 (2004) 709–719.
- [29] R.C. Bataller, Effects of heat source/sink, radiation and work doneby deformation on flow and heat transfer of a viscoelastic fluidover a stretching sheet, *Comput Math Appl* 53 (2007) 305–316.
- [30] R. Muhammad, M.I. Khan, M. Jameel, N.B. Khan, Fully developed Darcy-Forchheimer mixed convective flow over a curved surface with activation energy and entropy generation, *Comput. Meth. Prog. Biomed.* 188 (2020).
- [31] H. Waqas, Sami Ullah Khan, M.M. Bhatti, M. Imran, Significance of bioconvection in chemical reactive flow of magnetized Carreau-Yasuda nanofluid with thermal radiation

- and second-order slip, *Journal of Thermal Analysis and Calorimetry* 140 (2020) 1293–1306.
- [32] M.Y. Malik, T. Salahuddin, A. Hussain, S. Bilal, MHD flow of tangent hyperbolic fluid over a stretching cylinder: Using Kellerbox method, *Journal of Magnetism and Magnetic Materials* 395 (2015) 271–276.
- [33] Basavarajappa Mahanthesh, Giulio Lorenzini, Feteh Mebarek Oudina, Isac Lare Animasaun, Significance of exponential space- and thermal-dependent heat source effects on nanofluid flow due to radially elongated disk with Coriolis and Lorentz forces, *Journal of Thermal Analysis and Calorimetry* volume 141, pages37–44(2020).
- [34] B. Mahanthesh, Magnetohydrodynamic flow of Carreau liquid over a stretchable sheet with a variable thickness: The biomedical applications, *Multidiscipline Modeling in Materials and Structures* 16 (5) (2020) 1277–1293.
- [35] B.J. Gireesha, B. Mahanthesh, K.L. Krupalakshmi, Hall effect on two-phase radiated flow of magneto-dusty-nanoliquid with irregular heat generation/consumption, *Results in Physics* 7 (2017) 4340–4348.
- [36] Basavarajappa Mahanthesh, Nagavangala Shankarappa Shashikumar, Giulio Lorenzini, Heat transfer enhancement due to nanoparticles, magnetic field, thermal and exponential space-dependent heat source aspects in nanoliquid flow past a stretchable spinning disk, *J Therm Anal Calorim* (2020), <https://doi.org/10.1007/s10973-020-09927-x>.
- [37] B. Mahanthesh, B.J. Gireesha, S.A. Shehzad, A. Rauf, P.B. SampathKumar, Nonlinear radiated MHD flow of nanoliquids due to a rotating disk with irregular heat source and heat flux condition, *Physica B: Condensed Matter* 537 (15) (May 2018) 98–104.
- [38] S.J. Liao, Beyond perturbation: introduction to the homotopy analysis method, *Chapman and Hall, Boca Raton*, 2003.
- [39] M. I. Khan, F. Alzahrani, A. Hobiny, Heat transport and nonlinear mixed convective nanomaterial slip flow of Walter-B fluid containing gyrotactic microorganisms, *Alex. Eng. J.*, 59, 1761–1769.
- [40] M.S. Hashmi, N. Khan, Sami Ullah Khan, M.M. Rashidi, A Mathematical model for mixed convective flow of chemically reactive Oldroyd-B fluid between isothermal stretching disks, *Results in Physics* 7 (2017) 3016–3023.
- [41] M. Ijaz Khan, Faris Alzahrani, Aatef Hobiny, Zulfiqar Ali, Estimation of entropy optimization in Darcy-Forchheimer flow of Carreau-Yasuda fluid (non-Newtonian) with first order velocity slip, *Alexandria Engineering Journal* 59 (2020) 3953–3962, <https://doi.org/10.1016/j.aej.2020.06.057>.
- [42] R.A.V. Gorder, E. Sweet, K. Vajravelu, Analytical solutions of a coupled nonlinear system arising in a flow between stretching disks, *Appl. Math. comput.* 216 (2010) 1513–1523.